

Influence of finite thickness and stiffness on cellular adhesion-induced deformation of compliant substrata

John M. Maloney, Emily B. Walton, Christopher M. Bruce, and Krystyn J. Van Vliet*

Department of Materials Science and Engineering, Massachusetts Institute of Technology, Cambridge, Massachusetts 02139, USA

(Received 16 July 2008; published 29 October 2008)

Thin, mechanically compliant coatings commonly serve as substrata for adherent cells in cell biology and biophysics studies, biological engineering applications, and biomedical device design. The deformation of such a coating at the cell-substratum interface defines the link between cellular traction, substratum stiffness, and the chemomechanical feedback mechanisms responsible for cellular mechanosensitivity. Here we apply elasticity theory to investigate how this deformation is affected by the finite thickness of such a cell substratum. The model idealizes a cellular adhesion site (e.g., a focal adhesion) as a circular area of uniform tangential traction, and compares the deformation of a compliant semi-infinite material to that of a coating of the same material supported by a rigid base. Two parameters are identified and considered: center displacement (as a measure of adhesion site displacement) and normal strain gradient (as a measure of adhesion site distortion). The attenuation of these parameters provides two measures for the influence of a finite coating thickness and underlying rigid base on cell-mediated deformation of the compliant substratum. A dimensionless term in the resulting solutions connects the coating thickness to the characteristic size of the adhesion sites. This relation, and calculations of the minimum thickness at which the rigid base is practically undetectable by an adherent cell, are supported by existing experimental literature and our observations of the projected area of fibroblasts adhered to polyacrylamide hydrogel coatings with various thicknesses atop relatively rigid glass. The model thus provides a tool for estimating the effective stiffness sensed by a cell attached to a compliant coating. We also identify and consider conceptualizations of critical thickness, or minimum suitable thickness for an application, which depend on both the frame of reference and the cell behavior of interest. The appropriate usage of different definitions resolves the disparity in values reported in the literature. Finally, the distinction between adhesion site displacement and distortion noted in this model could be useful in designing substrata to elucidate the controlling mechanisms of cellular mechanosensing.

DOI: [10.1103/PhysRevE.78.041923](https://doi.org/10.1103/PhysRevE.78.041923)

PACS number(s): 87.10.Pq, 87.17.Rt

I. INTRODUCTION

Tissue cells are generally adherent, anchoring to adjacent surfaces through discrete sites of relatively weak, noncovalent interactions (see Fig. 1). Patches of transmembrane integrin molecules mechanically link the cell to the extracellular matrix (ECM) and the external environment; these adhesion sites are sometimes further classified as either focal complexes or focal adhesions or contacts depending on their size, state of development, and characteristic participating proteins [1,2]. At these locations, actomyosin contraction within the cell can result in stress exerted against the substratum [3,4]. In turn, the substratum supplies an equal and opposite stress at the cell adhesion sites (ignoring inertial effects), such that the cell and substratum each deform. The amount of substratum surface deformation influences cell behavior in a process known as mechanosensitivity [5–8]. Cells receive information about their mechanical environment from the coupling between stress applied by the cell at adhesion sites and the resulting deformation, including induced biochemical changes, at these sites.

Cell behavior studies have been performed on various two-dimensional (2D) substrata to explore mechanosensitivity, quantify adhesion traction, or mimic *in vivo* ECM. Often, the substratum consists of a compliant coating attached to

stiffer supports because the material is too compliant to handle easily [6,9,10]. [Here we distinguish between compliant (stiff) and soft (hard) designations; the first describes resistance to elastic or reversible deformation, the second,

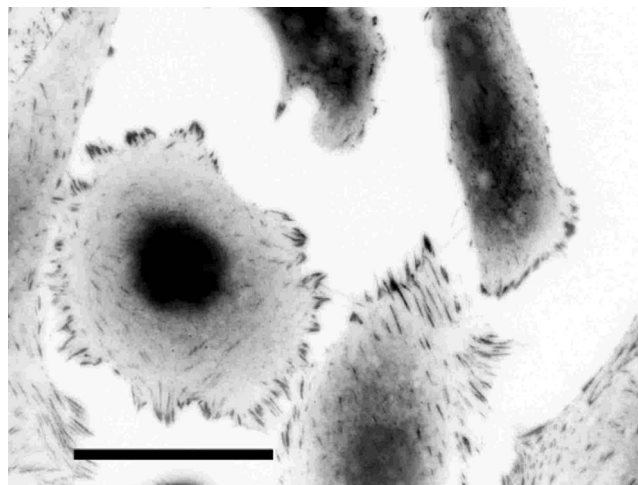


FIG. 1. Epifluorescence optical micrograph (negative image) of 3T3 fibroblasts, cultured on glass and fixed and stained for the focal adhesion adaptor protein vinculin (dark areas are the antivinculin antibody). Discrete vinculin features, often appearing at the periphery of the cells, correspond to adhesion sites between the cell and the adjacent surface. Scale bar=50 μm .

*krystyn@mit.edu

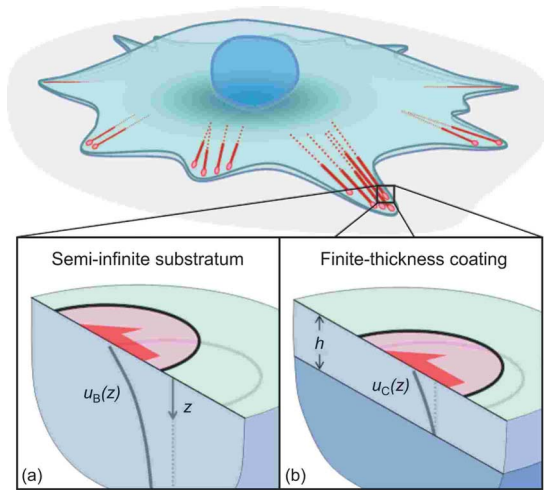


FIG. 2. (Color online) Schematic of adherent cell attached to (a) a half space, or semi-infinite substratum and (b) a coating of thickness h of the same material grafted to a rigid base. Adherent cells are contractile, exerting tangential traction on adhesion sites, here idealized as circular areas. The circular surface outlines indicate the undeformed and deformed positions and boundaries of the adhesion sites. Traction-induced deformation is attenuated by the presence of the rigid base; the displacements u_B and u_C , respectively, correspond to the Boussinesq, or semi-infinite substratum, solution and the finite coating solution, as described in the text. Note that the coating covers the rigid base and serves as a substratum for the adherent cell.

plastic or permanent deformation.] Additionally, layers of more than $1 \mu\text{m}$ thickness may be unavailable due to processing limitations (e.g., layer-by-layer deposition of polyelectrolyte multilayers [11,12]) or undesirable due to a need for optical transparency. This second consideration is important in cell traction microscopy, in which the motion of substratum-embedded beads or surface features is used to estimate the traction stresses exerted by cells [13–16].

A thin compliant coating attached to a comparably stiff base may present a very different mechanical environment to the cell than the bulk properties of the coating material would suggest (see Fig. 2). Therefore, a question arises concerning the influence of an underlying rigid base on the mechanical behavior of a compliant coating. Our goal is to investigate this question and also to determine the minimum coating thickness that can be approximated as a semi-infinite region. This minimum thickness could be considered a “critical thickness” in applications where it is undesirable for the rigid base to influence mechanical response. We present a model based on elasticity theory that describes how the cellular traction-induced surface deformation of a compliant coating is affected by the presence of an underlying rigid base. This effect has been investigated for the case of deflections far from the adhesion site by approximating regions of tangential traction as point forces [10]; however, we are interested in the surface deformation of the coating within the boundaries of the adhesion site where direct molecular mechanical transfer occurs. This adhesion site deformation has not previously been examined to our knowledge. We explore the case of a circular area of uniform shear stress; however,

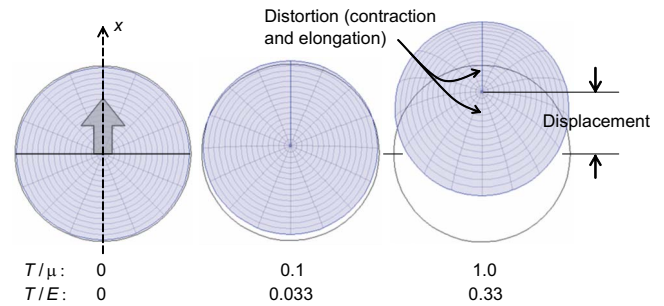


FIG. 3. (Color online) Displacement and distortion of circular area of applied tangential traction with increasing shear-stress-to-substratum-stiffness ratio; substratum Poisson’s ratio $\nu=0.5$. The deformation is calculated for a tangential traction T and substratum shear modulus μ or Young’s elastic modulus E by using equations derived in the text.

the model can be adapted to accommodate more complex geometry and stress distributions.

The model connects surface deformation to coating thickness and provides a tool for researchers to estimate an effective stiffness in cases where semi-infinite geometry is not attainable due to considerations such as processing, optical clarity, or cost. This method of calculating an effective stiffness can also be applied to conditions *in vivo*, where support structures such as the basement membrane or areolar connective tissue may be sufficiently thin to produce a multilayer mechanical response to adherent, epithelial-type cells [17]. We evaluate this model through observations of cell behavior on compliant coatings with various thicknesses and by considering the existing literature describing cell behavior on substrata with a range of stiffnesses and thicknesses.

Additionally, we investigate the discrepancy between values of critical thickness in the literature, which vary by one to two orders of magnitude both theoretically and experimentally. We conclude that several distinct and valid definitions of critical thickness h_c exist, depending on whether the deformation location of interest occurs at the adhesion site (as is the case with cell mechanosensitivity) or at a distance from multiple adhesion sites (as is the case with cell traction microscopy). The existence of different suitable definitions for different applications explains the disparity in literature reports. These definitions are further found to depend in different ways on the mechanical stiffness of the material from which the coating is synthesized.

II. MODEL

When a cell applies traction at an adhesion site, the underlying material deforms according to the mechanical properties of that material. An example of this deformation is illustrated in Fig. 3, in which the adhesion site is idealized as a circular area with radius a undergoing tangential traction, or shear stress [18,19]. A circular adhesion site area is especially amenable to analysis in our model due to its axisymmetry. Adhesion sites at cell-substrata interfaces, often visualized by immunofluorescent staining of actin-binding adaptor proteins, can appear approximately circular on very compliant materials ($E < 1 \text{ kPa}$) but appear generally irregu-

lar or elongated on stiffer substrata [6,20,35]. It is therefore noted that the circular area assumption represents a simplification of the actual adhesion site geometry.

Adhesion sites comprise a dense aggregate of transmembrane integrin receptors linked to the termini of actin filaments through a collection of adaptor proteins, a multimolecular structure sometimes termed an adhesion plaque. The uniform tangential traction assumed by our model represents the average shear stress due to the actomyosin contraction of generally parallel cytoskeletal filaments, as mediated by the compliant ($E \approx 1-10$ kPa) plaque [21]; this shear stress is in reality transmitted to the extracellular material via many discrete ECM ligand-integrin receptor pairs within the adhesion site. We will initially assume that this shear stress acts on a uniform half space, or semi-infinite region; this model will then be modified by assuming the existence of a perfectly rigid base under a coating of thickness h of the original material. This coating serves as the substratum of the adherent cell.

We therefore explore two geometries, as shown in Fig. 2. In case I, shear stress is applied to a finite region on the surface of a substratum consisting of a semi-infinite region occupying $0 \leq z < \infty$. In case II, shear stress is applied to a finite region on the surface of a finite-thickness coating that occupies $0 \leq z \leq h$ and is perfectly bonded to a perfectly rigid base occupying $h < z < \infty$. We define our coordinate system so that z points downward into the substratum and x corresponds to the direction of tangential loading. All materials are assumed to be isotropic, homogeneous, and linearly elastic. Additionally, only a single adhesion site is considered in this model; it is assumed that the traction-related deformation response due to other adhesion sites is negligible compared to the response due to the site of interest. The suitability of these assumptions is considered in Appendix A.

We investigate the effects of incorporating a rigid base on two modes of deformation. The first is the attenuation of

x -direction displacement, specifically at the center of the circle. The second is the attenuation of contraction and elongation in different regions of the circular area as shown in Fig. 3. We are interested in this distortion because of the importance of material gradients and molecular spacing in theories of adhesion site behavior at the molecular level. The two effects are analyzed separately in the following sections and termed “displacement” and “distortion.” We characterize displacement by the distance that the center of the circle S moves in the x direction. Distortion is quantified by the normal strain, or amount of contraction or elongation of the adhesion site at the coating surface. Since the value of the normal strain is zero at the center of the circle, we look instead at the first derivative of strain to characterize this effect.

An effective stiffness for a given compliant coating is then acquired by dividing the actual bulk stiffness by a normalized deformation factor we derive, which varies from zero to one according to the dimensionless ratio h/a , or the ratio of the coating thickness to the adhesion site radius.

A. Case I: Semi-infinite substratum

We first derive the equations governing the deformation of a semi-infinite region representing a bulk material or very thick coating. The calculated displacement and distortion values will serve as baselines when we incorporate the effects of an underlying rigid base. We use the subscript B to denote deformation related to the Boussinesq solution [22], which is employed in case I.

1. Displacement

In elasticity theory, a point force is coupled to a displacement field by the Green’s tensor. For an isotropic half space with a surface point force acting at (x_0, y_0) the surface Green’s tensor $\mathbf{G}_B(x, y, x_0, y_0)$ is [10,22]

$$\mathbf{G}_B = \frac{1}{2\pi\mu} \begin{pmatrix} \frac{2-\nu}{2r} + \frac{\nu(\hat{x}^2 - \hat{y}^2)}{2r^3} & \frac{\nu\hat{x}\hat{y}}{r^3} & -\frac{(1-2\nu)\hat{x}}{2r^2} \\ \frac{\nu\hat{x}\hat{y}}{r^3} & \frac{2-\nu}{2r} - \frac{\nu^2(\hat{x}^2 - \hat{y}^2)}{2r^3} & -\frac{(1-2\nu)\hat{y}}{2r^2} \\ \frac{(1-2\nu)\hat{x}}{2r^2} & \frac{(1-2\nu)\hat{y}}{2r^2} & \frac{1-\nu}{r} \end{pmatrix}, \quad (1)$$

where ν is Poisson’s ratio, $\mu = E/2(1+\nu)$ is the shear modulus, and E is Young’s elastic modulus, and

$$\hat{x} = x - x_0, \quad \hat{y} = y - y_0, \quad r = \sqrt{\hat{x}^2 + \hat{y}^2}. \quad (2)$$

Because Eq. (1) diverges at the location of the applied point force ($r \rightarrow 0$) [16,19], and we are interested in the deflections specifically at an adhesion site, we build on this result by integrating over a finite area S :

$$\mathbf{u}_B(x, y) = \iint_S \mathbf{G}_B(\hat{x}, \hat{y}) \mathbf{T} dS_0, \quad (3)$$

where $\mathbf{u}_B = (u_B \ v_B \ w_B)^T$ and \mathbf{T} is the local traction.

From the assumption of tangential loading and the definition of the coordinate system we have $\mathbf{T} = (T \ 0 \ 0)^T$. Let us assume that S is a circular region with radius a and centered at the origin. The displacement at any arbitrary point inside

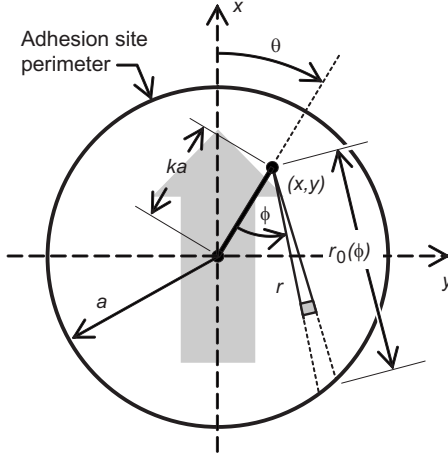


FIG. 4. Schematic for integrating the deflection due to a tangential traction in the x direction around an arbitrary interior point (x, y) . The adhesion site is idealized as a circular area with radius a .

the circle is found by integrating as shown in Fig. 4 and adapted from Saada's treatment of circular normal loading [23]:

$$\mathbf{u}_B(k, \theta) = \frac{T}{2\pi\mu} \times \int_0^{2\pi} \int_0^{r_0(\phi)} \begin{pmatrix} \frac{1 - \nu + \nu \cos^2(\theta - \phi)}{r} \\ \frac{\nu \sin(\theta - \phi) \cos(\theta - \phi)}{r} \\ \frac{(1 - 2\nu) \sin(\theta - \phi)}{2r} \end{pmatrix} r dr d\phi, \quad (4)$$

where

$$r_0(\phi) = a(k \cos \phi + \sqrt{1 - k^2 \sin^2 \phi}) \quad (5)$$

and we have used

$$\hat{x} = x - x_0 = r \cos(\theta - \phi), \quad \hat{y} = y - y_0 = r \sin(\theta - \phi). \quad (6)$$

After evaluating the integrals, the displacement field $\mathbf{u}_B(k, \theta)$ is

$$\mathbf{u}_B = \frac{Ta}{\mu} \begin{pmatrix} \frac{2 - \nu}{\pi} \mathcal{E}(k) + \frac{\nu \cos 2\theta}{3\pi k^2} [(2 - k^2) \mathcal{E}(k) - 2(1 - k^2) \mathcal{K}(k)] \\ \frac{\nu \sin 2\theta}{3\pi k^2} [(2 - k^2) \mathcal{E}(k) - 2(1 - k^2) \mathcal{K}(k)] \\ \frac{k(1 - 2\nu) \cos \theta}{4} \end{pmatrix}, \quad (7)$$

where k represents the normalized radial distance and $\mathcal{K}(k)$ and $\mathcal{E}(k)$ are the complete elliptic integrals of the first and second kind, respectively. The surface deformation of the circular area is shown in Fig. 3 for different ratios of T to μ and T to E . As a reference point, the traction exerted by adhesion sites of adherent cells has been experimentally determined to be approximately 5 kPa except at the smallest sites [14,24].

The x -direction displacement u_B is $Ta(2 - \nu)/2\mu$ at the center. The y and z displacements v_B and w_B , respectively, are zero at the center of the circle and average to zero over the area circumscribed by the circle.

The average u_B displacement within the circular area is

$$u_{B,av} = \frac{1}{\pi} \int_0^{2\pi} \int_0^1 u_B k dk d\theta = \frac{4Ta(2 - \nu)}{3\pi\mu}, \quad (8)$$

which is roughly 85% of the center displacement. From this value we can determine the strain energy stored in the substratum by a force-distance calculation to be $4T^2 a^3 (2 - \nu)/3\mu$.

It is also useful to consider an effective spring constant for substratum surface displacement,

$$k_{\text{eff}} = \frac{F}{u_B(0,0)} = \frac{2\pi\mu a}{2 - \nu} = \frac{\pi E a}{(1 + \nu)(2 - \nu)}, \quad (9)$$

to link this model with the spring constant calculations made by researchers working with cells adhered to compliant posts or pillars [24–26]. Micropillars have been designed to have a spring constant of approximately 1–20 nN/ μm . This range translates to a Young's elastic modulus of 0.7–14 kPa on a flat, semi-infinite compliant substratum undergoing tangential traction at an adhesion site with radius 1 μm .

2. Distortion

We would also like to investigate the distortion of the adhesion site circle. The normal strain characterizes the amount of contraction on the side of positive x , the side corresponding to the direction of applied tangential traction, and elongation of the side of negative x (see Fig. 3). The normal strain in the x direction ($\theta=0$) within the circle can be calculated from Eq. (4) as

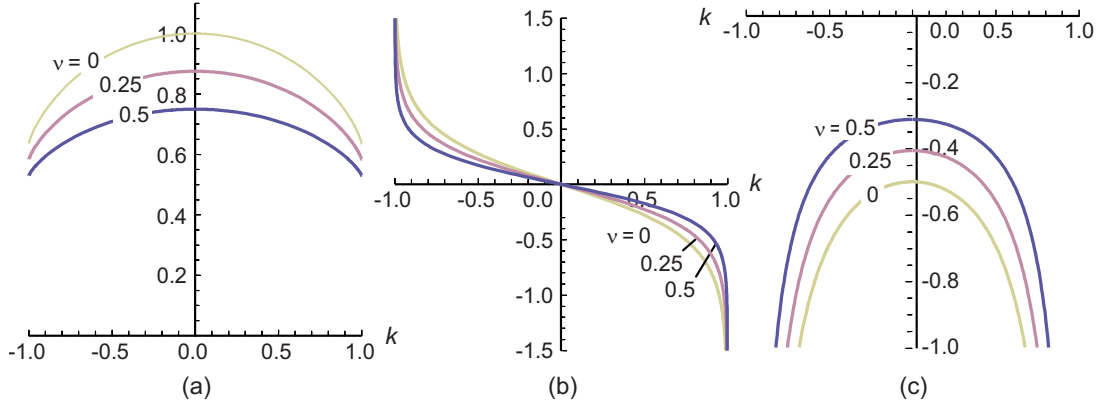


FIG. 5. (Color online) Normalized (a) surface displacement $u_B \mu / Ta$, (b) normal strain $\epsilon_{xx} \mu / T$, and (c) distortion (normal strain gradient) $(\mu/T) d\epsilon_{xx} / dk$ plotted as functions of k , the normalized radial distance to the adhesion site center, for three values of substratum Poisson's ratio ν (0, 0.25, 0.5) along the x axis ($\theta=0$). A discontinuity in strain and its derivative exists at $k=1$ (or $r=a$); we therefore focus on quantifying effects at the center of the circle.

$$\epsilon_{xx,B} = \frac{1}{a} \left(\frac{\partial u_B}{\partial k} \right) = \frac{T}{2\pi\mu a} \int_0^{2\pi} \frac{\partial r_0(\phi)}{\partial k} (1 - \nu + \nu \cos^2 \phi) d\phi. \quad (10)$$

This normal strain is zero at the center of the circle, which is the most convenient point to use (see Fig. 5). We therefore differentiate again to quantify the rate of transition from contraction at positive x to elongation at negative x . This parameter is used to quantify distortion:

$$\frac{\partial \epsilon_{xx,B}}{\partial k} = \frac{T}{2\pi\mu a} \int_0^{2\pi} \frac{\partial^2 r_0(\phi)}{\partial k^2} (1 - \nu + \nu \cos^2 \phi) d\phi. \quad (11)$$

At the center of the circular area of traction, the distortion is $-T(4-3\nu)/8\mu$; this value is negative because the normal strain ϵ_{xx} at the surface changes from positive to negative in the direction of positive x , as shown in Fig. 5. In this evaluation we have used the identities

$$\lim_{k \rightarrow 0} r_0(\phi) = a, \quad \lim_{k \rightarrow 0} \frac{\partial r_0(\phi)}{\partial k} = a \cos \phi, \quad (12)$$

$$\lim_{k \rightarrow 0} \frac{\partial^2 r_0(\phi)}{\partial k^2} = -a \sin^2 \phi.$$

We have now identified the characteristic displacement and distortion values $u_B(0,0) = Ta(2-\nu)/2\mu$ and

$\partial \epsilon_{xx,B}(0,0) / \partial k = -T(4-3\nu)/8\mu$, respectively, as baselines for comparison with the finite-thickness coating results derived in the following section.

B. Case II: Finite-thickness coating

We now assume that a perfectly bonded, rigid base exists under a compliant coating at a depth h . We use the C (coating) subscript for these parameters, but note that this coating serves as the cell substratum. Thus, an additional boundary condition $\mathbf{u}_C = \mathbf{0}$ at $z=h$ applies. There are at least two existing analytical methods for incorporating the effect of an underlying base. We describe two here, the methods of Yue [27] and Fabrikant [28]. Yue's method utilizes Fourier integral transforms in a backward transfer matrix approach to calculate the stresses and displacements in a multilayered isotropic half space subject to surface traction. Merkel *et al.* have presented experimental support for Yue's solution [10]. Fabrikant's method involves image forces that produce an infinite sum of reciprocals and solves a single transversely isotropic coating atop a rigid base. Here, we utilize Yue's approach and show Fabrikant's approach to be equivalent in Appendix B.

1. Displacement

In Yue's approach, the Green's tensor relating deformation and traction $\mathbf{G}_C(x,y,x_0,y_0)$ is [27]

$$\mathbf{G}_C = \frac{1}{2\pi} \int_0^\infty \begin{pmatrix} -\Phi_1 J_0 + \frac{\hat{x}^2 - \hat{y}^2}{r^2} \Phi_2 J_2 & \frac{2\hat{x}\hat{y}}{r^2} \Phi_2 J_2 & \frac{\hat{x}}{r} \Phi_{13} J_1 \\ \frac{2\hat{x}\hat{y}}{r^2} \Phi_2 J_2 & -\Phi_1 J_0 - \frac{\hat{x}^2 - \hat{y}^2}{r^2} \Phi_2 J_2 & \frac{\hat{y}}{r} \Phi_{13} J_1 \\ -\frac{\hat{x}}{r} \Phi_{31} J_1 & -\frac{\hat{y}}{r} \Phi_{31} J_1 & -\Phi_{33} J_0 \end{pmatrix} d\rho, \quad (13)$$

where

$$\Phi_1 = \frac{1}{2}[\Phi_{11}(\rho h) + \Phi_{22}(\rho h)], \quad \Phi_2 = \frac{1}{2}[\Phi_{11}(\rho h) - \Phi_{22}(\rho h)], \quad (14)$$

Φ represents a collection of characteristic terms to be defined below, and $J_m = J_m(\rho r)$ is the Bessel function of order m . The dummy variable ρ used in integration corresponds to the conjugate of distance in the Fourier-transformed domain.

The relevant terms in the portion of the Green's tensor \mathbf{G}_{i1} relating displacements to a tangential point force $\mathbf{T} = (T \ 0 \ 0)^T$ are calculated by Yue's method to be

$$\Phi_{11}(\rho h) = \frac{1}{\mu} \left(\frac{(1-\nu)[3-4\nu-4\rho h e^{2\rho h} - (3-4\nu)e^{4\rho h}]}{(3-4\nu)(1+e^{4\rho h}) - 4\nu + 2(5+2\rho^2 h^2 - 12\nu + 8\nu^2)e^{2\rho h}} \right), \quad (15a)$$

$$\Phi_{22}(\rho h) = \frac{1}{\mu} \left(\frac{1 - e^{2\rho h}}{1 + e^{2\rho h}} \right), \quad (15b)$$

$$\Phi_{31}(\rho h) = \frac{1}{\mu} \left(\frac{2e^{2\rho h}(2\rho^2 h^2 + 8\nu^2 - 10\nu + 3) - (8\nu^2 - 10\nu + 3)(1 + e^{4\rho h})}{2[(3-4\nu)(1 + e^{4\rho h}) + 2e^{2\rho h}(2\rho^2 h^2 + 8\nu^2 - 12\nu + 5) - 3]} \right), \quad (15c)$$

where μ is the shear modulus, ν is Poisson's ratio, and h is the coating thickness.

It can be verified that

$$\Phi_1(0) = \Phi_2(0) = \Phi_{31}(0) = 0, \quad (16)$$

which satisfies the condition of zero displacement when the coating thickness h is zero, and that

$$\lim_{h \rightarrow \infty} \Phi_1 = -\frac{2-\nu}{2\mu}, \quad \lim_{h \rightarrow \infty} \Phi_2 = \frac{\nu}{2\mu}, \quad \lim_{h \rightarrow \infty} \Phi_{31} = -\frac{1-2\nu}{2\mu}, \quad (17)$$

which, considering that the Bessel function integrals are normalized, recovers the half-space solution for an infinitely thick coating. The Φ terms are related to those given by Merkel *et al.* for pointlike adhesion sites for the analysis of cell traction microscopy and are presented here for clarity. Note that, in Merkel *et al.*'s notation, Φ_1 and Φ_2 are equivalent to $\mu\Phi_1 + (2-\nu)/2$ and $\mu\Phi_2 - \nu/2$, respectively, in Yue's and our notation.

We first calculate the x -direction displacement due to uniform traction applied over a finite area S for the case with an underlying rigid base, as part of our program of comparing deformation in cases I and II. This displacement $u_C(x, y)$ is

$$u_C = T \int \int_S G_{11,cd} dS_0 \quad (18a)$$

$$= \frac{T}{2\pi} \int \int_S \int_0^\infty \left(-\Phi_1 J_0 + \frac{x^2 - y^2}{r^2} \Phi_2 J_2 \right) d\rho dS_0. \quad (18b)$$

If we integrate over a circular area around the center, the second term in the integrand is zero:

$$u_C(0,0) = -\frac{T}{2\pi} \int_0^{2\pi} \int_0^a \int_0^\infty \Phi_1(\rho h) J_0(\rho r) d\rho r dr d\phi \quad (19a)$$

$$= -Ta \int_0^\infty \frac{1}{\rho} \Phi_1 \left(\frac{\rho h}{a} \right) J_1(\rho) d\rho. \quad (19b)$$

The dimensionless ratio h/a provides a connection between coating thickness and adhesion size that is discussed later in the context of critical thickness. It is useful to define the dimensionless factor U_1 that represents the attenuation of the x -direction displacement u at the center of the circle due to the presence of an underlying rigid base such that $u_C(0,0) = U_1(h/a)u_B(0,0)$. We can therefore write the normalized displacement $U_1(h/a)$ as

$$U_1 = -\frac{2\mu}{2-\nu} \int_0^\infty \frac{1}{\rho} \Phi_1 \left(\frac{\rho h}{a} \right) J_1(\rho) d\rho \quad (20a)$$

$$= 1 - \frac{2}{2-\nu} \int_0^\infty \frac{1}{\rho} \left[\mu \Phi_1 \left(\frac{\rho h}{a} \right) + \frac{2-\nu}{2} \right] J_1(\rho) d\rho, \quad (20b)$$

where the second expression in Eq. (20) is more amenable to numerical evaluation. Merkel *et al.* have noted that convergence of these types of integrals is improved if the semi-infinite region solution is taken outside the integral, leaving the integrand to represent the difference between this solution and the finite-thickness coating solution [10].

The dependence of U_1 on the ratio h/a is shown for three values of Poisson's ratio in Fig. 6(a). As h/a becomes large, U_1 approaches unity (100%) and the adhesion site center displacement is unattenuated and nearly the same on a compliant coating of thickness h as it would be on a semi-infinite substratum of the same material. As h/a becomes very small, U_1 approaches zero and the adhesion site center displaces as it would on a rigid substratum; that is, it does not displace at all. A consequence of this smooth transition is the need to specify a practical percentage when considering how deep a cell can "feel" (that is, the coating thickness that corresponds to a detectable change in cell behavior). In order to characterize adhesion site normalized displacement, we choose key

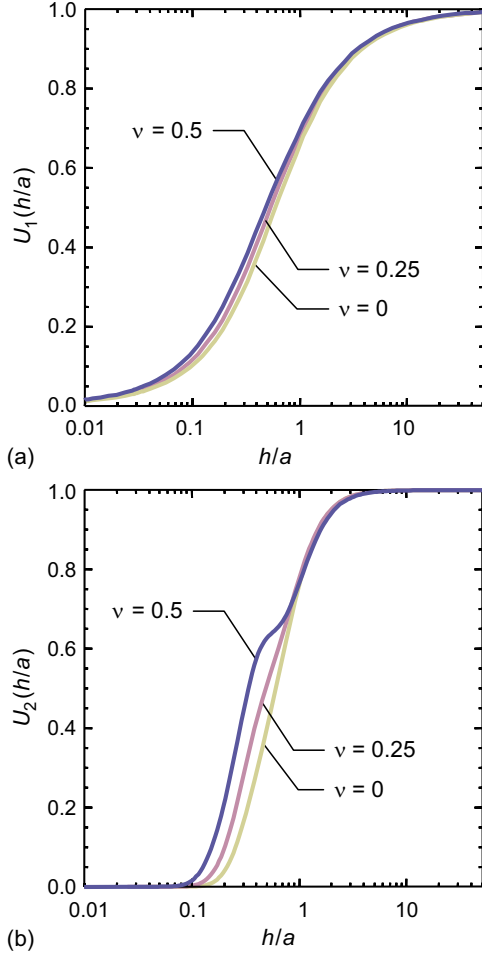


FIG. 6. (Color online) (a) Normalized coefficient $U_1(h/a)$ associated with the center displacement of a circular adhesion site of radius a due to the presence of an underlying rigid base at depth h as a function of h/a for three values of substratum Poisson's ratio ν (0, 0.25, 0.5). (b) Normalized coefficient $U_2(h/a)$ associated with the distortion of the same circular adhesion site. As the coating thickness $h \rightarrow \infty$, U_1 and U_2 approach unity, and the displacement and distortion approach that of the semi-infinite region solution. As h approaches zero, the displacement and distortion approach zero, representing complete attenuation of deformation due to the constraint of the rigid base.

values of $U_1(h/a)$ to be {10%, 50%, 90%}, which correspond to $h/a = \{0.075, 0.485, 3.42\}$ for $\nu = 0.5$. The 90% value, which is equivalent to 10% attenuation, serves as a reasonable definition of critical thickness h_c for this mode.

The typical radii of adhesion sites such as focal adhesions is on the order of $1 \mu\text{m}$ [1]. Our model therefore predicts that the adhesion site displacement is barely attenuated ($U_1 \approx 100\%$) due to the presence of a rigid base under a cell-substratum coating for h values of several micrometers or more. Note that this estimate is independent of the coating material stiffness E , due to the stated definition of U_1 . An interpretation of this result is that, for substratum thicknesses exceeding several micrometers, the rigid base is undetectable via cell mechanosensory mechanisms that respond to adhesion site displacement.

2. Distortion

We now consider the attenuation in distortion due to the presence of an underlying rigid base. We start at Eq. (18b). Let $F(\rho h, \rho r) = -\Phi_1 J_0 + \Phi_2 J_2 \cos 2\phi$. Then

$$u_C = \frac{T}{2\pi} \int_0^{2\pi} \int_0^{r_0(\phi)} \int_0^\infty F(\rho h, \rho r) d\rho r dr d\phi, \quad (21)$$

$$\begin{aligned} \varepsilon_{xx,C} &= \frac{1}{a} \left(\frac{\partial u_C}{\partial k} \right) \\ &= \frac{T}{2\pi a} \int_0^{2\pi} \frac{\partial r_0(\phi)}{\partial k} r_0(\phi) \int_0^\infty F(\rho h, \rho r_0(\phi)) d\rho d\phi, \end{aligned} \quad (22)$$

$$\begin{aligned} \frac{\partial \varepsilon_{xx,C}}{\partial k} &= \frac{1}{a} \left(\frac{\partial^2 u_C}{\partial k^2} \right) \\ &= \frac{T}{2\pi a} \int_0^\infty \int_0^{2\pi} \left\{ \left[\frac{\partial^2 r_0}{\partial k^2} r_0 + \left(\frac{\partial r_0}{\partial k} \right)^2 \right] \right. \\ &\quad \times F(\rho h, \rho r_0(\phi)) + r_0 \left(\frac{\partial r_0}{\partial k} \right) \\ &\quad \left. \times \frac{\partial}{\partial k} [F(\rho h, \rho r_0(\phi))] \right\} d\phi d\rho. \end{aligned} \quad (23)$$

Again, we let the normalized radius k approach zero and apply the limits in Eq. (12) to give

$$\begin{aligned} \frac{\partial \varepsilon_{xx,C}(0,0)}{\partial k} &= \frac{Ta}{2} \int_0^\infty \left(\Phi_2(\rho h) J_2(\rho a) + a\rho \Phi_1(\rho h) J_1(\rho a) \right. \\ &\quad \left. + \frac{a\rho}{4} \Phi_2(\rho h) [J_1(\rho a) - J_3(\rho a)] \right) d\rho \end{aligned} \quad (24a)$$

$$= \frac{T}{2} \int_0^\infty \rho \Phi_1 \left(\frac{\rho h}{a} \right) J_1(\rho) + \Phi_2 \left(\frac{\rho h}{a} \right) J_A(\rho) d\rho \quad (24b)$$

where $J_A = (\rho/4)J_1(\rho) + J_2(\rho) - (\rho/4)J_3(\rho)$. This equation can be shown to reduce to the half-space solution by letting $h \rightarrow \infty$ and by using the identities

$$\int_0^\infty J_n d\rho = 1, \quad \int_0^\infty \rho J_n d\rho = n \quad (25)$$

for $n = 1, 2, 3$.

As before, we can define a normalized coefficient by $\partial \varepsilon_{xx,C}(0,0) / \partial k = U_2(h/a) \partial \varepsilon_{xx,B}(0,0) / \partial k$. The parameter U_2 represents the attenuation of distortion (the gradient of the x -direction normal strain) by the presence of the underlying rigid base:

$$U_2(h/a) = -\frac{4\mu}{4-3\nu} \int_0^\infty \rho \Phi_1 \left(\frac{\rho h}{a} \right) J_1(\rho) + \Phi_2 \left(\frac{\rho h}{a} \right) J_A(\rho) d\rho \quad (26a)$$

$$\begin{aligned}
&= 1 - \frac{4}{4-3\nu} \int_0^\infty \rho \left[\mu \Phi_1 \left(\frac{\rho h}{a} \right) + \frac{2-\nu}{2} \right] J_1(\rho) \\
&\quad + \left[\mu \Phi_2 \left(\frac{\rho h}{a} \right) - \frac{\nu}{2} \right] J_A(\rho) d\rho. \quad (26b)
\end{aligned}$$

As in the case of U_1 , the second equation for U_2 here is more amenable to numerical evaluation.

The dependence of U_2 on the ratio h/a is shown for three values of Poisson's ratio in Fig. 6(b). The coefficient U_2 , like U_1 , asymptotically approaches zero and unity for very small and very large values of h/a , respectively. To enable an estimate of the critical thickness h_c for cell mechanosensory mechanisms that detect adhesion site distortion, key values of $U_2(h/a)$ for $\nu=0.5$ are {10%, 50%, 90%} at $h/a = \{0.156, 0.341, 1.58\}$. The coating thickness or rigid base depth predicted to attenuate distortion by 10% for an adhesion site radius of 1 μm is 1.58 μm , about half the corresponding value for U_1 . Therefore, calculations involving both deformation modes predict that an underlying rigid base under a coating thickness of more than several micrometers is undetectable by adherent cells that respond to one or both of these modes. In our discussion below, we contrast the use of U_1 and U_2 for specific cases relevant to cell adhesion and mechanosensitivity.

C. Estimates of U_1 for finite-thickness substrata

It is desirable to have simple analytical expressions or approximations for the normalized deformation functions U_1 and U_2 . The relationship $U_1(h/a)$ when $\nu=0.5$ is well fitted by the approximate equation

$$U_1(h/a) \approx 1 - 0.77e^{-1.9h/a} - 0.23e^{-0.23h/a} \quad (27)$$

with an error of less than 4% for $h/a > 0.1$. Although this empirical equation fits well, it has no physical basis.

A closed-form approximation with physical basis can be developed by the following reasoning. By comparison of the deflection beneath the center of the adhesion site in cases I and II as shown in Fig. 2, it can be seen that the displacements u_C and u_B , which have been calculated analytically, are similar in the range $0 \leq z \leq h$ except for a constant offset. Therefore, an approximation to u_C can be found by subtracting the deflection u_B at $z=h$ from the deflection u_B at the surface, and a closed-form approximation to U_1 is

$$U_1^*(z/a) = 1 - \frac{u_B(0,0,z)}{u_B(0,0,0)}. \quad (28)$$

To make this approximation, we must calculate the deflection within the substratum directly underneath the center of the circular area, which can be found from the more general expression of $G_{B,11}(x,y,x_0,y_0,z)$ for arbitrary z [29]:

$$G_{B,11} = \frac{1}{4\pi\mu} \left[\frac{1}{R} + \frac{\hat{x}^2}{R^3} + (1-2\nu) \left(\frac{1}{R+z} - \frac{\hat{x}^2}{r(R+z)^2} \right) \right], \quad (29)$$

where $R = \sqrt{r^2 + z^2}$ and positive z is again measured downward into the substratum.

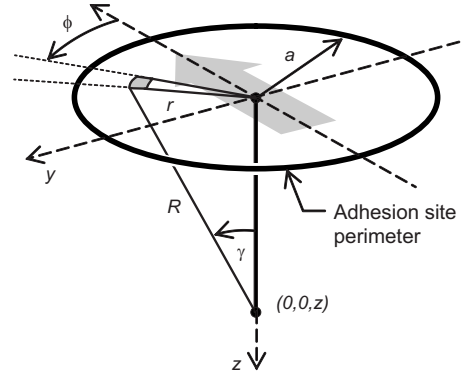


FIG. 7. Schematic for integration of the deflection at an arbitrary depth under the center of a circular area of tangential traction in the x direction.

We restrict our focus to the deformation under the center so that $\hat{x}=x$ and $\hat{y}=y$. The deflection at arbitrary depth under the center of the circle is (see Fig. 7)

$$u_B(0,0,z) = T \int_0^{2\pi} \int_0^a G_{B,11} r dr d\gamma. \quad (30)$$

We make the variable substitutions $r=R \sin \phi$ and $R = z \sec \phi$ so that $x = -R \cos \gamma \sin \phi$ and $dr = z \sec^2 \phi d\phi$:

$$\begin{aligned}
u_B(0,0,z) = \frac{Tz}{4\pi\mu} \int_0^{2\pi} \int_0^{\tan^{-1}(a/z)} &\left[\left(\frac{1}{\sec \gamma} + \frac{1-2\nu}{1+\sec \gamma} \right) \right. \\
&+ \cos^2 \gamma \left(\frac{\sin^2 \phi}{\sec \phi} - (1-2\nu) \frac{\sin^2 \phi \sec \phi}{(1+\sec^2 \phi)^2} \right) \\
&\left. \times \tan \phi \sec^2 \phi d\phi d\gamma. \quad (31)
\end{aligned}$$

From this we obtain

$$u_B(0,0,z) = \frac{T}{4\mu} \left(\frac{z^2}{\sqrt{a^2+z^2}} + (4-2\nu)\sqrt{a^2+z^2} - (5-2\nu)z \right). \quad (32)$$

It can be verified by using the approximations

$$\sqrt{a^2+z^2} \approx \begin{cases} a + z^2/2a & \text{if } z \ll a, \\ z + a^2/2z & \text{if } z \gg a. \end{cases} \quad (33)$$

that this equation simplifies to the point force case $Ta^2(3-2\nu)/8\mu z$ when a is small and to the surface displacement solution $Ta(2-\nu)/2\mu$ as z goes to zero.

Equations (28) and (32) are combined as

$$\begin{aligned}
U_1^*(z/a) = 1 - \frac{1}{2a(2-\nu)} \\
\times \left(\frac{z^2}{\sqrt{a^2+z^2}} + (4-2\nu)\sqrt{a^2+z^2} - (5-2\nu)z \right). \quad (34)
\end{aligned}$$

Subtracting the at-depth deflection $u_B(0,0,0)$ from the surface deflection $u_B(0,0,z)$ in this manner produces an exact answer only in the case of $a \rightarrow \infty$, which is equivalent to a shear stress applied over the entire coating surface. For a

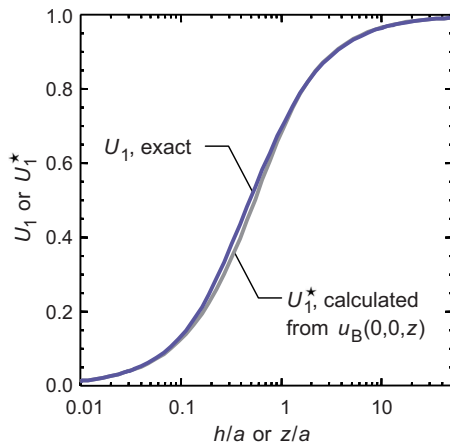


FIG. 8. (Color online) Exact numerical evaluation of $U_1(h/a)$ in Eq. (20) compared to approximation $U_1^*(z/a)$ in Eq. (34); substratum Poisson's ratio $\nu=0.5$ for both calculations.

finite a , this estimate leaves the boundary condition $\mathbf{u}_C = (u_C v_C w_C)^T = 0$ at $z=h$ unsatisfied except at $(0,0,h)$. However, this discrepancy appears to have only minor consequences, as shown in Fig. 8. The approximation has the benefit of deviating by less than 10% from the exact solution when $\nu=0.5$. Additionally, both the exact solution and the approximation converge to $4h/3a$ for small h/a when $\nu=0.5$, so that the relative error converges to zero for these conditions.

We have not obtained a comparably simple and physically motivated expression for U_2 , and thus consideration of distortion effects requires numerical evaluation of Eq. (26).

III. MATERIALS AND METHODS

A. Preparation of polyacrylamide thin gel films

Cell behavior was investigated on coatings of various thicknesses. Polyacrylamide films were used as model elastic substrata, prepared on silanized, amine-derivitized glass coverslips following the well-established protocol of Wang *et al.* [30]. Polyacrylamide prepolymer solutions were made by mixing 625 μl of 40% acrylamide solution and 325 μl of 2% bis solution (Bio-Rad Labs, Hercules, CA), 50 μl of 1M 4-(2-hydroxyethyl)-1-piperazineethanesulfonic acid (HEPES) (Cambrex, Walkersville, MD), and 1500 μl of purified water. The prepolymer solution was activated with 30 μl of a 10% ammonium persulfate solution (Bio-Rad Labs, Hercules, CA) and 20 μl n,n',n',n'-tetramethylethylenediamine (Bio-Rad Labs, Hercules, CA).

The gel thickness h was controlled via two methods. Gels of thickness $h > 5 \mu\text{m}$ were prepared by sandwiching a known volume of activated prepolymer solution between two glass coverslips [30]. Gels of thickness $h < 5 \mu\text{m}$ were prepared with activated prepolymer solution containing polystyrene beads of diameters of 0.3, 0.6, 1.1, 3, and 6 μm (Sigma-Aldrich, St. Louis, MO), according to established protocols [31]. The bead-containing solution was sandwiched between two glass coverslips and clamped until polymerization was complete.

Fully polymerized gels were functionalized for cell attachment by room temperature incubation for 2 h in a gelatin (Becton Dickinson 214340, Sparks, MD) solution (1 mg/ml in phosphate-buffered saline), followed by rinsing in purified water. Gelatin adsorption resulted in an undetectable thickness increase as measured by atomic force microscopy (AFM) profiling over fresh scratches in polyacrylamide gels of nominal 3 μm thickness and similar formulation (8% acrylamide) to that used in cell culture experiments (5% acrylamide). The standard deviations of absolute thickness among replicate measurements was 500 nm in both the unfunctionalized and gelatin-adsorbed gels (data not shown). Gels were stored in 50 mM HEPES buffer at 4 $^\circ\text{C}$.

B. Characterization of thin polyacrylamide hydrogel coatings

Gel thicknesses were verified by AFM profiling or, for the thicker gels ($h > 20 \mu\text{m}$), calibrated optical microscopy. Gel stiffness was determined via AFM-enabled indentation (Molecular Imaging, now Agilent, Santa Clara, CA) using cantilevers of user-calibrated stiffness $k_c=0.03 \text{ N/m}$ (Veeco, Camarillo, CA). Force-distance indentation responses were analyzed to determine Young's elastic modulus E by using Igor Pro analysis software, following a previously described model [32]. The mean and standard deviation of indentation-measured Young's elastic modulus for polyacrylamide gels was $5.6 \pm 1.1 \text{ kPa}$ for gels of thickness $h=60 \mu\text{m}$ indented to maximum indentation depth $\Delta=800 \text{ nm}$.

C. Cell culture and proliferation assays

NIH-3T3 fibroblasts (ATCC: CRL-1658) were cultured in Dulbecco's Modified Eagle Medium (Gibco/Invitrogen 11885, Carlsbad, CA) with 10% bovine calf serum (HyClone, Logan, UT). Experiments were performed in duplicate. The cells were seeded at a surface density of 5000 cells/ cm^2 onto gelatin-coated gels atop glass cover slips. After 24 h, the culture medium was exchanged and the adherent cells imaged with an optical microscope in phase contrast (Olympus IX51, Center Valley, PA).

D. Observation and analysis

Cell areas were analyzed by using IMAGEJ (NIH, Bethesda, MD); one researcher used this software to trace the cell areas on images randomly labeled by a colleague. Only the areas of free (noncontiguous) cells were measured due to the possibility of contact inhibition.

IV. RESULTS AND DISCUSSION

A. Comparison with experiment through the calculation of effective stiffness

One consequence of finite substratum thickness is that cell traction-induced displacements may be reduced via mechanical contributions of the rigid support, anthropomorphized as the cell "feeling" a stiffer substratum than would be expected from the known elastic properties of the substratum material and possibly adopting new cell morphologies or behaviors consistent with a stiffer external environment. Our model

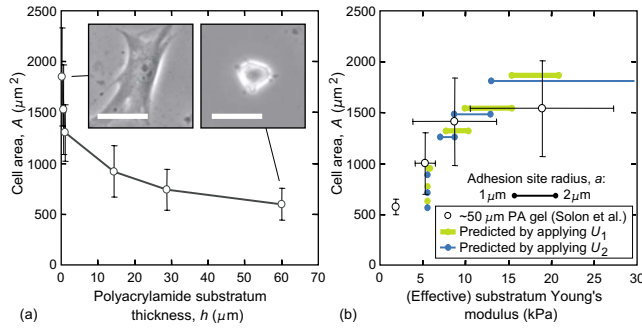


FIG. 9. (Color online) (a) Cell area A for 3T3 fibroblasts adhered to polyacrylamide gels with Young's elastic modulus $E = 5.6$ kPa and a range of thicknesses fabricated on glass. The reduction in thickness of a compliant coating on an underlying rigid base results in increased effective stiffness and an increase in spread cell area. Error bars represent standard error ($n \geq 47$). Inset: phase contrast photographs of cells adhered to relatively thin and thick coatings of the same formulation of polyacrylamide (scale bars = 50 μm). (b) The same data plotted as a function of effective Young's elastic modulus (calculated by dividing the actual Young's elastic modulus by the deformation function U_1 or U_2) for two assumed adhesion site radii, 1 and 2 μm , and compared to Solon *et al.*'s measurements of fibroblast area on relatively thick polyacrylamide gels [33]. In (b), cell area error bars are omitted and the predictions from U_1 and U_2 are slightly offset vertically for clarity.

predicts that an effective shear modulus can be calculated by dividing the coating shear modulus by a thickness-dependent normalized function $U_i(h/a)$ (U_1 or U_2):

$$\mu_{\text{eff}} = \frac{\mu}{U_i(h/a)}, \quad (35)$$

where μ_{eff} and μ can be replaced with E_{eff} and $E = 2\mu(1 + \nu)$, respectively, because ν is assumed to be constant (and equal to 0.5 for the compliant coatings discussed in this section).

To test these predictions directly, we conducted new experiments that documented the projected area of NIH-3T3 fibroblasts adhered to polyacrylamide hydrogel coatings on comparably rigid glass supports. The use of polyacrylamide on glass is well established for cell mechanotransduction studies; however, a systematic study using a range of well-defined coating thickness values has not previously been performed.

Fibroblast projected areas for different polyacrylamide thickness values are shown in Fig. 9(a). This cell-spreading area A was most sensitive to changes in coating thickness for thicknesses of less than several micrometers, as predicted by our model. Above this thickness, there is little change in cell area, suggesting that the underlying glass base is nearly undetectable by cell mechanosensory mechanisms.

Cell area as a function of substratum thickness (A - h data) can be transformed into cell area as a function of effective stiffness (A - E_{eff} data) by using Eq. (35); U_i is evaluated by using the measured polyacrylamide bulk Young's elastic modulus E and an assumption of adhesion site radius a with Poisson's ratio $\nu = 0.5$. The transformed relationship is shown in Fig. 9(b) and compared to a previously reported relation-

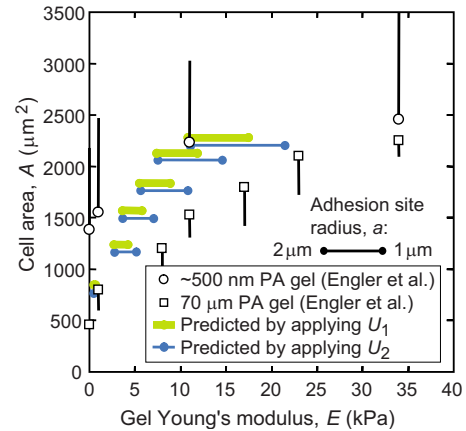


FIG. 10. (Color online) Open symbols are cell area measurements on 70 μm (squares) and 500 nm (circles) compliant polyacrylamide (PA) hydrogel coatings as reported by Engler *et al.* [36]; data and vertical error bars are as published in [36]. Closed symbols are the result of applying our model's functions U_1 and U_2 to the 70 μm data to predict cell area on a 500 nm film. The predictions from U_1 and U_2 are slightly offset vertically for clarity, and the horizontal range of U_1 and U_2 is due to the range of assumed adhesion site radii a from 1 to 2 μm .

ship for 3T3 fibroblasts on thick (50 μm) polyacrylamide films [33]. The stiffness-area trend is also similar to reported trends for 3T3 fibroblasts on other thick (≥ 50 μm) polyacrylamide films [6,34] and also for kidney epithelial cells [6], endothelial cells [34], smooth muscle cells [31,35], and mesenchymal stem cells [36].

We have also applied our model to existing experimental data reported by Engler *et al.* that consist of area measurements of mesenchymal stem cells on compliant polyacrylamide coatings of thickness $h = 70$ μm and 500 nm bonded to a rigid underlying base [36]. Engler *et al.* considered the 70 μm films to be essentially semi-infinite based on earlier experiments, and we concur, based on our model's predictions of $U_1 \approx U_2 \approx 1$ for large values of h/a .

Our model can operate on thickness and stiffness specifications in such a way as to predict thick-coating behavior from thin-coating behavior, and vice versa. In application to the data reported by Engler *et al.*, we used our model to predict thin-coating (500 nm) cell behavior based on the reported thick-coating (70 μm) behavior by multiplying the measured stiffness values of the thick coating by $U_1(h/a)$ and $U_2(h/a)$ for adhesion site radii $a = 1$ and 2 μm . The larger number of experimentally measured points (higher data density) in these thick-coating results made this operation more favorable than the reverse operation. Both Engler *et al.*'s experimental data and our model's predictions of cell area on a 500-nm-thick film are shown in Fig. 10. Note that the only input to our model was the substratum stiffness in the semi-infinite case (taken to be the stiffness reported for the thick-coating case) and the assumed adhesion site radii a . We find our model to be a good predictor of the change in cell behavior (here, cell area A) resulting from the use of a thinner vs a thicker coating of the same material.

In both examples of calculating effective stiffness (fibroblasts and mesenchymal stem cells), the predictions from

using functions U_1 and U_2 are similar enough to prevent us from drawing any conclusions on whether the cells used either displacement- or distortion-related feedback to sense substratum stiffness.

An additional test of our model would be its application to more parameters than just the projected area of adhered, spread cells. A complex behavior that is plausibly modulated by mechanical stiffness of substrata would be ideal. For example, motility can vary according to substratum stiffness in a biphasic manner [35]; our model predicts that this relationship would be shifted if a thick, essentially semi-infinite coating were replaced by a thin coating on an underlying rigid base. Finally, we are also exploring thickness gradients in coatings of a single material as a way of simulating variations in stiffness, in anticipation of comparison with experimental observations of cell behavior on coatings with stiffness gradients [37].

B. The existence of several definitions of critical thickness: How deep can a cell feel?

A range of estimates exists in the literature concerning the minimum suitable coating thickness in 2D cell culture experiments. This issue arises, for example, in cell traction microscopy and in observations of cell behavior of substrata of various stiffness. A justified interpretation of critical thickness is required not just for basic scientific experiments of mechanosensitivity, but also to address the range of engineered cell functions achievable with synthetic substrata and device coatings. Reported estimates have varied by one to two orders of magnitude both theoretically and experimentally. Scaling arguments have been used to support critical thickness estimates from several micrometers to tens of micrometers: for example, Dembo and Wang [13] and Balaban *et al.* [14] connected the minimum suitable thickness to the magnitude of ($\approx 1 \mu\text{m}$) surface displacements, arguing that the minimum coating thickness should at least be large compared to displacements. Butler *et al.* used scaling arguments to estimate a minimum suitable thickness; they modeled a focal adhesion as a circular area of traction (as we do), but then changed to using the length of an entire cell as a characteristic length to be compared with coating thickness [18]. Yang *et al.* repeated this reasoning, proposing that a $70 \mu\text{m}$ film may not be sufficiently thick to prevent a $50\text{-}\mu\text{m}$ -long fibroblast from being affected by an underlying rigid base [38]. However, Schwartz *et al.* reasoned that it is the focal adhesion size rather than the cell size that should be compared to coating thickness [16].

Experimental estimates of critical thickness have also varied. Del Álamo concluded from spectral energy density data that critical thickness is dependent on cell size and is in the tens of micrometers [39]. However, Engler *et al.* found no detectable difference in smooth muscle cell behavior on $h=5$ and $70 \mu\text{m}$ polyacrylamide gel coatings on glass and concluded that cells cannot feel as deep as $5 \mu\text{m}$. They first compared the sensing depth to cell height [31], but later compared it to adhesion site size [36].

Thus, both scaling arguments and experimental observations encompass a variety of characteristic cell dimensions in

determining purported critical thickness. Analytical estimates are most useful if also predictive of experimental observations, and we believe that the experimental findings of del Álamo *et al.* and Engler *et al.* can be resolved by considering whether the surface displacements of interest lie at a distance from the adhesion site, as is the case in cell traction microscopy, or very close to the adhesion site, which is the only region the cell can interrogate. The same finite-thickness-coating elasticity model predicts that the attenuation from the rigid base in the first case is dependent on h/r (Merkel *et al.*'s calculation from Yue's general solution [10]) and in the second case is dependent on h/a [derived in this work as Eqs. (20) and (26)]. These two dimensionless quantities arise naturally from a model of tangential traction applied to the surface of a coating grafted to a rigid base, and they predict different values of critical thickness depending on the application. The value of r can be one to two orders of magnitude larger than that of a , and this ratio reflects the difference in critical thickness estimates of del Álamo *et al.* and Engler *et al.*

In the process of considering these examples of a minimum suitable thickness, we have identified other possible definitions of a critical thickness h_c in cell biophysics studies on compliant coatings. A critical thickness can be said to correspond to the depth that a cell can feel, and it is therefore important to identify and compare definitions to avoid misunderstandings and to clarify data on cell traction-induced substratum deformation. These definitions are listed in Table I. Of particular interest is the different ways that these characteristic depths depend on a material property such as coating stiffness. Depending on one's criterion (strain cutoff, attenuation of remote bead displacement, attenuation of adhesion site deformation), the depth may increase, decrease, or remain unchanged as a result of increasing stiffness.

We suggest that the definitions in Table I are ordered according to relevance in the design of finite-thickness coatings intended to elicit a predicted response of adherent cells or, alternatively, to assess which mode of adhesion site deformation most strongly regulates cell mechanosensitivity. The first two items are less relevant in this ordering. The arbitrary nature of the strain definition reduces its usefulness, and, as we discussed earlier, the critical thickness for cell traction microscopy is controlled by the distance from adhesion site to bead, a measurement of no significance in mechanosensitivity. The metrics of attenuation that we define in this work are more useful. It seems clear, for example, that a cell cannot feel an underlying base that is too far away to attenuate traction-induced surface deformation at an adhesion site. Finally, the last item in Table I may be the most relevant to cell behavior: a coating thickness that would produce a certain surface deformation. We include this definition because of the interesting consequence that the thickness would need to increase to maintain the same surface deformation as coating stiffness increases. This increase lies in contrast with the decrease in arbitrary strain depth, another critical thickness definition, following the same increase in coating stiffness. However, it is difficult to theorize further about this last definition of critical thickness without knowing more about the cell mechanosensory mechanism and what modes of substratum deformation constitute primary feedback to an adherent

TABLE I. Possible definitions of critical cell-sensing depth or coating thickness for adherent (traction-exerting) cells on 2D substrata.

Description of critical depth or thickness	Effect of increasing coating stiffness
Depth at which a certain strain ϵ_{xx} exists [2,40]	Decreases ($\propto\sqrt{T/\mu}$)
Coating thickness that attenuates cell traction microscopy measurements at a distance r by a certain percentage	Independent ($\propto r$)
Coating thickness that attenuates adhesion site displacement by a certain percentage (characterized by U_1) (this work)	Independent ($\propto a$)
Coating thickness that attenuates adhesion site distortion by a certain percentage (characterized by U_2) (this work)	Independent ($\propto a$)
Coating thickness that maintains a certain traction-induced surface displacement or distortion	Increases ($\propto f(\mu), \propto a$)

cell. Future experiments that consider the effects of finite coating thickness may help resolve this issue.

C. Displacement versus distortion

Two normalized deformation functions (U_1 and U_2) have been identified, and they are both functions of the dimensionless ratio h/a , indicating a coupling between characteristic depths and adhesion site size. U_1 is a measure of center displacement attenuation, and U_2 is a measure of distortion attenuation. Considering the deformation of the substratum as two separate modes, displacement and distortion, may help clarify models of adhesion site growth and stability. Displacement has long been regarded as an important parameter in elasticity-based models of focal adhesion behavior [41,42]. Other researchers have conjectured that the spacing of bound integrin molecules correlates with their binding affinity and lifetime, thereby influencing adhesion site growth and stability [21,43,44]. Distortion of the substratum adjacent to the adhesion area may affect this spacing.

It could be illuminating to consider existing or novel substrata that suppress either displacement or distortion to gauge the effect on adhesion site and cell morphologies. Consider, for example, substrata with compliant posts [24–26]. We predict that posts with spring constant $k=10$ nN/ μm displace like semi-infinite substrata with Young's elastic modulus $E=7$ kPa (assuming a circular area with radius 1 μm of tangential traction) but distort essentially like the bulk silicone with Young's elastic modulus of 2 MPa from which they were made. Would adhesion site morphology and protein recruitment correspond to that typically seen on the stiffer or less stiff material? The answer would provide insight into the nature of the cellular mechanosensory mechanism.

While the two normalized deformation functions U_1 (representing attenuation of center displacement) and U_2 (representing attenuation of distortion) represent possible ways of characterizing the influence of an underlying rigid base, and while adhesion site models in the literature appear to ascribe a mechanosensory mechanism to adhesion site displacement and/or distortion, there is nevertheless no assurance that

mechanosensation is affected by these parameters. The substratum stiffness feedback used by the cell may incorporate one or the other parameter, both parameters, or additional information not yet defined. It seems clear, however, that the feedback must incorporate some aspect of surface deformation of the 2D substratum on which the cell is attached.

As physical models of adhesion site growth and stability emerge, additional modes of deformation may be found to be important. Our model presents a method for calculating the attenuation due to finite coating thickness for any mode of deformation, by returning to the Green's tensors given in Eqs. (1) and (13) and calculating \mathbf{u}_B and \mathbf{u}_C .

D. Scope of model

We discuss here the scope of our model and its position in the field of adhesion site modeling. This work is meant to complement theories of focal adhesion formation and behavior, which often idealize the substratum as perfectly rigid [44,45]. Recent work has attempted to address variations in substratum stiffness and thickness [21]. However, considerations of substratum thickness are typically limited to analysis of the limiting cases of thin and thick coatings. Our model provides a quantitative link from very thin to semi-infinite coatings, in the form of the normalized deformation functions U_i . The calculations are not dependent on any particular theory of adhesion site formation and growth. In its calculation of an effective stiffness, the model is in agreement with Nicolas *et al.*'s general predictions that a thin, compliant extracellular matrix should lead to a similar behavior as a thick, stiffer ECM.

Assumptions of our model include the use of a single adhesion site shape (circular with radius a) and a constant tangential traction T . Since an elongated adhesion site morphology is generally observed for cells cultured on substrata of Young's elastic modulus E greater than approximately 1 kPa [6,20,35], this model sacrifices some physical accuracy in favor of ease of mathematical analysis. For cell types and/or substrata stiffness for which noncircular adhesion sites are observed, analytical or numerical solutions for non-

axisymmetric adhesion site shapes are possible but are beyond the scope of the current study. For example, elliptical areas of traction have been previously used to model adhesion sites on compliant substrata [10,16]. In the absence of an analytical solution of attenuated substrata deformation for traction over an ellipse, we speculate that the critical thickness would still be related to the adhesion site size, as shown in this work for circular areas, and that this characteristic length would be a function of the major and minor axes of the elliptical idealized shape rather than equivalent to the circle radius. Additionally, the tangential traction within an adhesion site also may not be constant and has been modeled as varying along its length [46]; however, data are not yet available to suggest a more accurate traction distribution. Furthermore, it should be emphasized that we are modeling the substratum distortion only, which is not necessarily equivalent to the more complex distortion behavior of adhesion site molecules.

Finally, the model does not inform the user of which function U_i to use; it only allows calculation of the attenuation of certain deformation parameters. As discussed earlier, we draw a distinction between two distinct deformation modes to prompt new exploratory experiments into cell mechanosensitivity.

V. CONCLUSIONS

For both fundamental studies of cellular mechanotransduction and applied studies of coatings intended to recapitulate tissue environments, it is important to understand the extent to which finite substrata thickness affects the mechanical resistance encountered via cellular traction at discrete adhesion sites. We have applied our continuum elasticity model and its distinction between adhesion site displacement (U_1) and distortion (U_2) to calculate the effective stiffness of thin substrata deformed via traction at adhesion sites. We verified that this thickness-defined effective stiffness rationalizes comparable cell areas observed for thick, stiff gels and thin, compliant gels in both previously reported experiments and our present results for fibroblasts on compliant polyacrylamide gels. The ability to describe and predict cell-level responses for substrata of varying stiffness and thickness in terms of effective substratum thickness should facilitate quantitative comparison among disparate experimental conditions as well as the effective design of coatings intended to represent a predefined mechanical environment to adhered cells. Further, we applied our model to rationalize the wide range of estimates for critical thickness h_c in the present literature, from the diameter of molecular complexes to the diameter of entire cells, in that each estimate depends on whether the perturbed property is defined relative to deformation within the cell or far from the cell. Each of these valid perspectives depends on cell-defined parameters (e.g., adhesion site radius or shear stress) and material-defined parameters (e.g., Young's elastic modulus). Thus, the model quantitatively connects the critical thickness definition most relevant in considerations of mechanosensitivity to the characteristic size of adhesion sites, a connection that has been observed in experiments and intuited through scaling arguments but not previously derived rigorously.

Practical applications of this model still require careful consideration of the purposes for which mechanically defined substrata are employed: Is one's goal to match *in vivo* levels of adhesion site displacement, of cell morphology, of substratum contraction, of maximal cell traction, and/or metabolic activity? For applications in which the substratum is intended to provide a well-defined mechanical environment that maintains a specified surface deformation, for example, our model shows that this critical thickness depends not only on substratum material stiffness but also on adhesion site radius. Of more general interest are the mechanisms by which this mechanical environment is converted to biochemical processes that alter cellular functions, and the extent to which these mechanisms depend separately (if at all) on the displacement and distortion of the multimolecular adhesion sites at which stress is transferred from the intra- to extracellular environments. The current model cannot resolve this important question based on available experimental data, but rather serves as a means to design and interpret future experiments that seek to define and leverage these primary feedback mechanisms.

ACKNOWLEDGMENTS

The authors acknowledge support from the National Defense Science and Engineering program (E.B.W.), from NSF (K.J.V.V.), and from the Arnold and Mabel Beckman Foundation (J.M.M. and K.J.V.V.).

APPENDIX A: QUALIFICATIONS FOR THE USE OF LINEAR ELASTICITY

The model described in this paper relies upon the assumptions of coating isotropy, homogeneity, and linear elasticity. These assumptions could become invalid if one or more of the following conditions apply.

(1) The characteristic length scale of (inevitable) material inhomogeneity is not negligible compared to the adhesion site radius. For example, polyacrylamide hydrogels, used in cell traction microscopy and in this work, consist of a hydrated network of polymer chains. The pore size (radius) of similar gel formulations to that used in this work is approximately 100 nm [47], which is small compared to adhesion site size. The *in vivo* basement membrane, which could be treated as a 2D substratum for adherent epithelial cells, consists of a meshwork of collagen fibers with branch points spaced at 45 nm [48]. The use of continuum theory is a reasonable assumption in our model for such materials. However, biomimetic scaffolds with pore sizes of several micrometers or more (e.g., collagen-glycosaminoglycan scaffolds for regeneration of connective tissue or skin [49]) would violate the continuum assumption, since a cell attached to one or more struts is expected to detect a composite mechanical response affected both by the material stiffness and the structural (bending) stiffness of the scaffold struts. Such structures are more appropriately modeled as cellular solids [49], as the present model assumes traction is exerted over a semi-infinite half space or a coating adhered to a relatively rigid support.

(2) The loading is sufficiently large to cause the material's stress-strain relationship to deviate from linearity. This factor is material dependent. We have focused mostly on polyacrylamide because of its widespread use in cell traction and mechanosensitivity experiments. Unfortunately, the experimental evidence that polyacrylamide is actually linear elastic for typical cell traction values is, to the best of our knowledge, unresolved by current experiments.

(3) The loading is sufficiently large to cause the geometry to change so that the assumption of loading direction is invalid, or the products of strains become non-negligible. An estimate of the point where geometrical changes prevent the accurate use of linear elasticity in analytical models of substratum deformation is the focus of current research employing large-displacement finite-element analysis.

(4) The loading from a single adhesion site is linear, but the aggregate loading from multiple sites exceeds the threshold of linear elastic behavior. A related issue is whether deformation from neighboring adhesion sites can be ignored compared to "self-deformation," an assumption of our model. This issue can be explored by considering a line of equally spaced (centers separated by na) adhesion sites of radius a as an idealization of the arrangement often found at the periphery of an adherent cell (see Fig. 1). The line is perpendicular to the x -direction tangential traction and extends along the y -axis. At the center of any particular site, the displacement due to the two nearest neighbor sites is

$$2\pi a^2 \frac{T}{2\pi\mu} \left(\frac{2-\nu}{2r} + \frac{\nu(x^2-y^2)}{2r^3} \right) = \frac{Ta}{n\mu}, \quad (\text{A1})$$

where we have treated the other sites as point forces for ease of calculation [19] and used $r=x=na$ and $\nu=0.5$. We compare this displacement to that caused by the tangential traction of the central adhesion site ($3Ta/4\mu$). For a spacing of $n=4$ (circular adhesion sites separated by equally sized spaces), the contribution from the two nearest neighbors alone is predicted to be one-third of the self-displacement. This is not a negligible amount, but neither does it exceed the self-displacement; the actual spacing may be more or less depending on the distribution of adhesion sites. We ignore this deformation from neighboring sites because of the considerable computational savings that results.

APPENDIX B: EQUIVALENCE OF FABRIKANT'S FORMULATION

We now address Fabrikant's solution [28], which relies upon the method of images. Fabrikant writes $G_{11,C}(x,y,x_0,y_0)$ in a form equivalent to

$$G_{11,C} = G_{11,B} + \frac{1}{2\pi\mu} \sum_{m=1}^{\infty} \left[\frac{1-\nu}{2} Q_m + (-1)^m \left(\frac{1}{\hat{r}(2m)} + \frac{\hat{x}^2 - \hat{y}^2}{\hat{r}(2m)[\hat{r}(2m) + 2mh]^2} \right) \right] \quad (\text{B1})$$

where $\hat{r}(\beta) = \sqrt{r^2 + (\beta h)^2}$ and Q_m is calculated by considering the boundary conditions in a calculation-intensive process [28]. For example, the first three terms in the case of $\nu=0.5$ are

$$Q_1 = -2f(2) - 4f'(2) - 4f''(2), \quad (\text{B2a})$$

$$Q_2 = 2f(4) + 8f'(4) + 16f''(4) + 16f'''(4) + 16f''''(4), \quad (\text{B2b})$$

$$Q_3 = -2f(6) - 12f'(6) - 36f''(6) - 64f'''(6) - 96f''''(6) - 64f^{(5)}(6) - 64f^{(6)}(6), \quad (\text{B2c})$$

where

$$f(\beta) = \frac{1}{\hat{r}(\beta)} - \frac{\hat{x}^2 - \hat{y}^2}{\hat{r}(\beta)[\hat{r}(\beta) + \beta h]^2} \quad (\text{B3})$$

and the derivatives indicated by f' , f'' , etc. are taken with respect to β .

By using an approach outlined by Fabrikant, we can show the equivalence of Yue's and Fabrikant's equations. We begin with Eq. (13) and rewrite Yue's Φ_{11} and Φ_{22} as

$$\begin{aligned} \Phi_{11} &= \frac{1-\nu}{\mu} \left(e^{-4\rho h} - 1 - \frac{4\rho h e^{-2\rho h}}{3-4\nu} \right) \\ &\times \sum_{n=0}^{\infty} \left(-e^{-4\rho h} - \frac{1+4\rho^2 h^2 + (3-4\nu)^2}{3-4\nu} e^{-2\rho h} \right)^n, \end{aligned} \quad (\text{B4})$$

$$\Phi_{22} = \frac{1}{\mu} (e^{-2\rho h} - 1) \sum_{n=0}^{\infty} (-e^{-2\rho h})^n. \quad (\text{B5})$$

These expressions can be evaluated term by term with the identities

$$\int_0^{\infty} (\rho h)^\alpha e^{-\beta\rho h} J_0(\rho r) d\rho = \left(-\frac{\partial}{\partial\beta} \right)^\alpha \frac{1}{\hat{r}(\beta)}, \quad (\text{B6})$$

$$\int_0^{\infty} (\rho h)^\alpha e^{-\beta\rho h} J_2(\rho r) d\rho = \left(-\frac{\partial}{\partial\beta} \right)^\alpha \left(\frac{r^2}{\hat{r}(\beta)[\hat{r}(\beta) + \beta h]^2} \right), \quad (\text{B7})$$

and are found to be equivalent to Eq. (B1).

- [1] B. Geiger and A. Bershadsky, *Curr. Opin. Cell Biol.* **13**, 584 (2001).
- [2] R. Krishnan, B. Oommen, E. Walton, J. Maloney, and K. Van Vliet, *Cell Adhesion Migration* **2**, 13 (2008).
- [3] C. Izzard and L. Lochner, *J. Cell. Sci.* **21**, 129 (1976).
- [4] K. Burridge, K. Fath, T. Kelly, G. Nuckolls, and C. Turner, *Annu. Rev. Cell Biol.* **4**, 487 (1988).
- [5] D. Choquet, D. Felsenfeld, and M. Sheetz, *Cell* **88**, 39 (1997).
- [6] R. Pelham, Jr. and Y. Wang, *Proc. Natl. Acad. Sci. U.S.A.* **94**, 13661 (1997).
- [7] D. Discher, P. Janmey, and Y. Wang, *Science* **310**, 1139 (2005).
- [8] S. Peyton, C. Ghajar, C. Khatiwala, and A. Putnam, *Cell Biochem. Biophys.* **47**, 300 (2007).
- [9] A. Engler, L. Bacakova, C. Newman, A. Hategan, M. Griffin, and D. Discher, *Biophys. J.* **86**, 617 (2004).
- [10] R. Merkel, N. Kirchgessner, C. Cesa, and B. Hoffmann, *Biophys. J.* **93**, 3314 (2007).
- [11] J. Mendelsohn, S. Yang, J. Hiller, A. Hochbaum, and M. Rubner, *Biomacromolecules* **4**, 96 (2003).
- [12] M. Thompson, M. Berg, I. Tobias, M. Rubner, and K. Van Vliet, *Biomaterials* **26**, 6836 (2005).
- [13] M. Dembo and Y. Wang, *Biophys. J.* **76**, 2307 (1999).
- [14] N. Balaban *et al.*, *Nat. Cell Biol.* **3**, 466 (2001).
- [15] K. Beningo and Y. Wang, *Trends Cell Biol.* **12**, 79 (2002).
- [16] U. Schwarz, N. Balaban, D. Riveline, A. Bershadsky, B. Geiger, and S. Safran, *Biophys. J.* **83**, 1380 (2002).
- [17] A. Shukla, A. Dunn, M. Moses, and K. Van Vliet, *Mech. Chem. Biosyst.* **1**, 279 (2004).
- [18] J. Butler, I. Tolic-Norrelykke, B. Fabry, and J. Fredberg, *Am. J. Physiol.: Cell Physiol.* **282**, 595 (2002).
- [19] B. Sabass, M. Gardel, C. Waterman, and U. Schwarz, *Biophys. J.* **94**, 207 (2008).
- [20] W. Guo, M. Frey, N. Burnham, and Y. Wang, *Biophys. J.* **90**, 2213 (2006).
- [21] A. Nicolas *et al.*, *Biophys. J.* **91**, 61 (2006).
- [22] J. Boussinesq, *Applications des Potentiels à l'Étude de l'Équilibre et du Mouvement des Solides Élastiques* (Paris: Gauthier-Villars, 1885).
- [23] A. Saada, *Elasticity Theory and Applications* (Krieger, Malabar, FL, 1993).
- [24] J. Tan, J. Tien, D. Pirone, D. Gray, K. Bhadriraju, and C. Chen, *Proc. Natl. Acad. Sci. U.S.A.* **100**, 1484 (2003).
- [25] O. du Roure, A. Saez, A. Buguin, R. Austin, P. Chavrier, P. Silberzan, and B. Ladoux, *Proc. Natl. Acad. Sci. U.S.A.* **102**, 2390 (2005).
- [26] A. Saez, A. Buguin, P. Silberzan, and B. Ladoux, *Biophys. J.* **89**, 52 (2005).
- [27] Z. Yue, *Q. J. Mech. Appl. Math.* **49**, 471 (1996).
- [28] V. Fabrikant, *Math. Proc. Cambridge Philos. Soc.* **138**, 173 (2005).
- [29] K. Johnson, *Contact Mechanics* (Cambridge University Press, Cambridge, MA, 1987).
- [30] Y. Wang and R. Pelham, Jr., *Methods Enzymol.* **298**, 489 (1998).
- [31] A. Engler, L. Richert, J. Wong, C. Picart, and D. Discher, *Surf. Sci.* **570**, 142 (2004).
- [32] J. Domke, and M. Radmacher, *Langmuir* **14**, 3320 (1998).
- [33] J. Solon, I. Levental, K. Sengupta, P. Georges, and P. Janmey, *Biophys. J.* **93**, 4453 (2007).
- [34] T. Yeung, P. Georges, L. Flanagan, B. Marg, M. Ortiz, M. Funaki, N. Zahir, W. Ming, V. Weaver, and P. Janmey, *Cell Motil. Cytoskeleton* **60**, 24 (2005).
- [35] S. Peyton and A. Putnam, *J. Cell Physiol.* **204**, 198 (2005).
- [36] A. Engler, S. Sen, H. Sweeney, and D. Discher, *Cell* **126**, 677 (2006).
- [37] C. Lo, H. Wang, M. Dembo, and Y. Wang, *Biophys. J.* **79**, 144 (2000).
- [38] Z. Yang, J. Lin, J. Chen, and J. Wang, *J. Theor. Biol.* **242**, 607 (2006).
- [39] J. del Álamo, R. Meili, B. Alonso-Latorre, J. Rodriguez-Rodriguez, A. Aliseda, R. Firtel, and J. Lasheras, *Proc. Natl. Acad. Sci. U.S.A.* **104**, 13343 (2007).
- [40] E. Walton, B. Oommen, and K. Van Vliet, in *Engineering in Medicine and Biology Society, 29th Annual International Conference of the IEEE*, 2007, edited by B. E. Layton (IEEE, Lyon, France, 2007).
- [41] I. Bischofs, *Proc. Natl. Acad. Sci. U.S.A.* **100**, 9274 (2003).
- [42] U. Schwarz, T. Erdmann, and I. Bischofs, *BioSystems* **83**, 225 (2006).
- [43] A. Nicolas, B. Geiger, and S. Safran, *Proc. Natl. Acad. Sci. U.S.A.* **101**, 12520 (2004).
- [44] A. Besser and S. Safran, *Biophys. J.* **90**, 3469 (2006).
- [45] T. Shemesh, B. Geiger, A. Bershadsky, and M. Kozlov, *Proc. Natl. Acad. Sci. U.S.A.* **102**, 12383 (2005).
- [46] D. Aroush and H. Wagner, *Adv. Mater. (Weinheim, Ger.)* **18**, 1537 (2006).
- [47] D. Holmes and N. Stellwagen, *Electrophoresis* **12**, 612 (1991).
- [48] P. Yurchenco and G. Ruben, *J. Cell Biol.* **105**, 2559 (1987).
- [49] B. Harley, J. Leung, E. Silva, and L. Gibson, *Acta Biomaterialia* **3**, 463 (2007).